American Journal of Pathology, Vol. 152, No. 1, January 1998

Experimental Autoimmune Encephalomyelitis in Mice Lacking Glial Fibrillary Acidic Protein Is Characterized by a More Severe Clinical Course and an Infiltrative Central Nervous System Lesion

Wolfgang Liedtke,* Winfried Edelmann,† Fung-Chow Chiu,‡ Raju Kucherlapati,† and Cedric S. Raine*§¶

From the Departments of Pathology, Molecular Genetics,† Anesthesiology,‡ Neurology,§ and Neuroscience,¶ Albert Einstein College of Medicine, Bronx, New York*

Insights into the role of the astrocyte intermediate filament protein, glial fibrillary acidic protein (GFAP), have only recently emerged with reports on subtle abnormalities in GFAP-deficient mice, including the documentation of defective long-term maintenance of central nervous system myelination. Here, we extend these observations by examining the astroglial response in GFAP$^{-/-}$ mice with autoimmune encephalomyelitis (EAE), a model for multiple sclerosis. Clinically, the monophasic disease was more severe in GFAP$^{-/-}$ mice than in wild-type littermates despite increased remyelination in the former. More in keeping with the clinical course was the observation of an infiltrative EAE lesion in GFAP$^{-/-}$ mice. GFAP$^{-/-}$ astrocytes had a reduced cytoarchitectural stability as evidenced by less abundant and irregularly spaced hemidesmosomes. The blunt GFAP$^{-/-}$ astrocyte processes possessed intermediate filaments consisting mainly of vimentin, though to a lesser degree than in the wild-type. In contrast, in wild-type littermates, GFAP was most abundant and nestin occurred at lower levels. Taken together, the present study introduces the novel concepts that GFAP plays an important role in the control of clinical disease associated with formation of a clearly defined edge to the EAE lesion and that GFAP is operative in the regulation of the intermediate filament components in reactive fibrillary astrogliosis. ***(Am J Pathol 1998, 152:251–259)***

Intermediate filaments (IF) are a group of cytoskeletal proteins commonly subgrouped into six classes based on IF-bearing cell type.[1,2] In the mammalian central nervous system (CNS), neurons contain three different types of neurofilaments. Astrocytes contain the IF glial fibrillary acidic protein (GFAP), some astrocytes and their precursors contain the IF vimentin, and CNS cells of an earlier developmental stage contain the embryonic IF nestin.[2–4] Vimentin-bearing astrocytes of the adult CNS are positive for both GFAP and vimentin, having cytoskeletal IF of mixed composition.[4] Outside the CNS, GFAP occurs in intestinal autonomic glial cells and in nonmyelinating Schwann cells.[5,6] Since its isolation in 1971 from a chronic multiple sclerosis (MS) plaque,[7] GFAP has been identified as a major constituent of reactive astrogliosis, a common reaction to a number of stimuli.[8] This reaction is generally considered detrimental; research into the properties and roles of GFAP has been driven by this view and by the ensuing rationale of down-regulating the gliotic response.[8] The role of GFAP *in vivo* has only recently become clearer after subtle anomalies in GFAP$^{-/-}$ mice[9–13] were described in several reports, one of which reported hydrocephalus, immature oligodendroglia and ongoing myelination in aging GFAP$^{-/-}$ mice, irregular CNS architecture including CNS vascularization, and an abnormal blood-brain barrier.[13]

In the present study, to evaluate possible additional abnormalities in GFAP$^{-/-}$ mice, experimental autoimmune encephalomyelitis (EAE) was induced to investigate the glial reaction in response to inflammatory stimuli. EAE is a Th_1 $CD4^+$ T-cell-mediated autoimmune disease of the CNS with clinical and neuropathological similarities to MS, an inflammatory demyelinating condition of the human CNS of unknown etiology.[14–16] In MS, recurrent disease activity leads to increased glial scarring that is associated with accumulating neurological deficit.[17]

Our results have revealed a novel role for GFAP *in vivo*—that GFAP is necessary for restricting the EAE lesion. Furthermore, clinical disease was more severe in GFAP$^{-/-}$ mice.

Supported by the National Institutes of Health grants NS 08952, NS 11920, and NS 07098; the National Multiple Sclerosis Society grants RG 1001-I-9; Feodor Lynen-Fellowship of the Alexander von Humboldt-Foundation, Bonn, Germany to W. Liedtke.

Accepted for publication October 17, 1997.

Address reprint requests to Dr. Wolfgang Liedtke, Howard Hughes Medical Institute, Department of Molecular Genetics, The Rockefeller University, Room # RRB 640, 1230 York Avenue, New York, NY 10021. E-mail: liedtkw@rockvax.rockefeller.edu.

Materials and Methods

Transgenic Mice

The generation of GFAP$^{-/-}$ mice has been described elsewhere.[13] The animals were of a mixed C57BL/6 × 129/Ola genetic background. Age- and sex-matched littermates were used as wild-type (wt) controls.

Induction of EAE

EAE was induced by active immunization with whole myelin in complete Freund's adjuvant. The mixed genetic background of the mice precluded passive transfer EAE. In view of the known resistance of C57BL mice to induction of EAE,[18] the following protocol was applied. Female mice, 6 to 8 weeks of age were injected subcutaneously into four sites at the tail base and the right and left flanks with 0.1 ml of an emulsion consisting of 13 mg of myelin/ml of saline and 670 μg of *Mycobacterium tuberculosis*/ml of incomplete Freund's adjuvant (Difco, Detroit, MI). Myelin was prepared from whole spinal cord of guinea pig according to the method of Norton and Poduslo.[19] On the day of immunization and on days 2 and 7 after immunization, 100 ng of Pertussis toxin (ICN, Costa Mesa, CA)/0.1 ml of saline were injected intravenously.

Clinical disease was scored on a scale from 0 to 5. Absence of disease scores a 0; tail weakness scores a 0.5; tail paralysis scores a 1; one hindlimb paretic scores a 2; paraplegic scores a 3; quadriplegic scores a 4; and moribund scores a 5. Mice were sampled either during the acute stage of the disease or in the remission phase.

Mice were perfused transcardially with either 2.5% glutaraldehyde in Millonig's buffer for embedding of the CNS in epoxy resin, with 10% neutral-buffered formalin for embedding of the CNS in paraffin, or with saline for protein extraction from the CNS in 8 mol/L urea for Western blotting.

Histopathology

For light microscopy, 1 μm of toluidine blue-stained epoxy sections were prepared by processing nine levels of CNS from optic nerve to sacral spinal cord plus spinal roots. The tissue was postfixed in osmic acid, dehydrated, and embedded in epoxy resin. Two sections of each level were graded by blinded observers on a scale of 0 to 4 for the presence and degree of cellular infiltrate, demyelination, remyelination, and Wallerian degeneration.

For electron microscopy, representative epoxy blocks from each group of animals were selected for acute and long-standing lesions. Thin sections were placed on 200 mesh copper grids, stained with lead citrate and uranyl acetate, and scanned in a Siemens 101.

For immunohistochemistry (IHC), paraffin- and plastic-embedded sections were used. The former were deparaffinized, pretreated either by trypsinization (0.1% trypsin (Sigma) in saline for 25′ at 37°C) or by autoclaving for 25′ in distilled water. Epoxy sections were deplasticized and etched by incubation in sodium ethoxide as described elsewhere.[13] Subsequently, sections were quenched in 0.3% H_2O_2, blocked with 10% normal goat serum/0.1% Triton X-100 for 2 hours, and incubated with primary antibody overnight at 4°C. The following primary antibodies were used: anti-GFAP (clone 18–0021, Zymed, San Francisco, CA) at 1:50; anti-vimentin (clone MAB 1681, Chemicon, Temecula, CA) at 1:20, anti-vimentin (clone MAB 1633, Chemicon; clone Vim3B4, Boehringer Mannheim, Indianapolis, IN; clone V-9, Sigma, St. Louis, MO) as a cocktail at 1:100 each; anti-nestin (clone Rat-401, Chemicon) at 1:50; and polyclonal rabbit antibodies specific for desmin (Chemicon) at 1:1000. Pretreatment by autoclaving was more suitable for GFAP and nestin; trypsinization increased specific staining for the other antibodies. The following negative controls were included: saline, isotype-specific antibody, and purified mouse immunoglobulin at a concentration equivalent to the primary antibody for monoclonals; nonspecific polyclonal antibody and normal rabbit serum (Dako, Carpenteria, CA), for polyclonal rabbit antibody. Detection of the primary antibodies was performed with the avidin-biotin complex method as described.[13] Stained sections were scored by blinded observers on a scale of 0 to 4 based on the abundance of positively staining cells and their processes. Four animals from each group of mice with long-standing EAE were used for semiquantitative grading. At least seven levels of formalin-fixed, paraffin-embedded spinal cord were analyzed.

Western Blotting

This was performed as described.[13] Briefly, proteins were extracted from different areas of the CNS with 8 mol/L urea/1 mmol/L proteinase inhibitor phenylmethylsulfonyl fluoride. Ten to 60 μg of total protein were loaded onto a denaturing 6 to 10% sodium dodecyl sulfate-polyacrylamide gel electrophoresis gel. Proteins were transferred by electroblotting onto nitrocellulose or polyvinylidene difluoride membranes and immunodetected with 4-chloro-1-naphtol as substrate for GFAP (anti-GFAP antibody, clone G-A-5, 1:500, Boehringer Mannheim) or with chemoluminescence (NEN Life Science Products, Boston, MA) for vimentin (anti-vimentin antibody, clone Vim3B4, 1:100, Boehringer Mannheim) and nestin (anti-nestin antibody, Rat-401, 1:250, Chemicon; rabbit anti-nestin[20] 1:10000, a gift from Dr. R. McKay, the National Institutes of Health, Bethesda, MD). For nestin immunoblotting, Triton X-100-insoluble, cytoskeletal protein fraction (prepared as described elsewhere[9]) of a p3 rat cerebellum and of a chronic relapsing EAE mouse spinal cord were included as positive controls. Proteinase inhibitor cocktail (Boehringer Mannheim) was added to the lysis buffer at 1 tablet/25 ml. Densitometry of specific bands was performed with the software program, NIH Image.

Statistical Analysis

A software program, Sigmastat (Jandel, San Rafael, CA), was applied to perform the Student's *t*-test, the Mann-Whitney *U* test, and Fisher's exact test for comparison between groups.

Table 1. Clinical Parameters of EAE in $GFAP^{-/-}$ and $GFAP^{+/+}$ Mice

Parameter	$GFAP^{-/-}$	$GFAP^{+/+}$	*P*
Incidence	13 of 17	12 of 21	n.s.
Mean cumulative disease score*	0.94 (0.25)	0.22 (0.094)	<0.0001
Maximum severity	1.41 (1.06)	0.81 (0.83)	0.094

*Mean cumulative disease score is calculated by forming the mean of the daily average clinical scores; given is the mean value, standard deviation in (parentheses).
n.s., not significant.

Results

Clinical Course Is More Severe in $GFAP^{-/-}$ Mice

A total of 38 animals were immunized; 17 $GFAP^{-/-}$ and 21 wt littermates. There was no difference in disease incidence as indicated by 13 of 17 $GFAP^{-/-}$ and 12 of 21 $GFAP^{+/+}$ mice developing clinical signs (Table 1). The monophasic, nonremitting disease course for all animals is shown in Figure 1A; the course for diseased animals is depicted in Figure 1B. EAE was more severe in $GFAP^{-/-}$ animals, although on the whole, the disease was mild in both groups. Worsened clinical course was highlighted by a significantly different mean cumulative disease score of 0.94 ($GFAP^{-/-}$) *versus* 0.22 ($GFAP^{+/+}$) ($P < 0.0001$, Mann-Whitney *U* test; Table 1). In addition, group-to-group comparison between day 20 and day 60 after immunization revealed 16 of 40 days to be significantly different between groups ($P < 0.05$; Table 1, Figure 1A). In this regard, it is of relevance that on day 43 after immunization, 5 $GFAP^{-/-}$ and 6 $GFAP^{+/+}$ animals were sampled (the most afflicted), leading to nonsignificant *P* values in the remainder. Other clinical parameters did not differ significantly between groups (Table 1). Mean values for disease onset (day 20.4 $GFAP^{-/-}$ *versus* day 20.9 $GFAP^{+/+}$) and maximum severity of EAE (1.41 $GFAP^{-/-}$ *versus* 0.81 $GFAP^{+/+}$) did not differ significantly between groups.

Light Microscopy—the EAE Lesion is Poorly Delineated in $GFAP^{-/-}$ Mice

The character of the CNS lesion in affected mice was inflammatory and demyelinating, which was similar to EAE lesions in other, susceptible mouse strains, and occurred in 14 of 17 $GFAP^{-/-}$ and 19 of 21 $GFAP^{+/+}$ animals. Most striking was the lesion edge that was well defined in wt littermates (Figure 2 b, d, and f), but conspicuously ill-defined and infiltrative in $GFAP^{-/-}$ mice (Figure 2 a, c, and e). This was the case for acute disease (Figure 2, a and b), but it was even more apparent in long-standing lesions (Figure 2, c and f). Standardized semiquantitative scoring for cellular infiltration, demyelination, remyelination, and wallerian degeneration revealed no statistically significant differences between groups (cellular inflammation 0.8 ± 0.41 for $GFAP^{+/+}$, 0.96 ± 0.56 for $GFAP^{-/-}$; demyelination 0.75 ± 0.58 for $GFAP^{+/+}$, 1.0 ± 0.64 for $GFAP^{-/-}$; remyelination 0.28 ± 0.21 for $GFAP^{+/+}$, 0.24 ± 0.15 for $GFAP^{-/-}$; Wallerian degeneration 0.78 ± 0.88 for $GFAP^{+/+}$, 1.6 ± 0.97 for $GFAP^{-/-}$, $P = 0.19$, Student's *t*-test), although there was a clear trend toward increased Wallerian degeneration in $GFAP^{-/-}$ animals (see also Figure 2e).

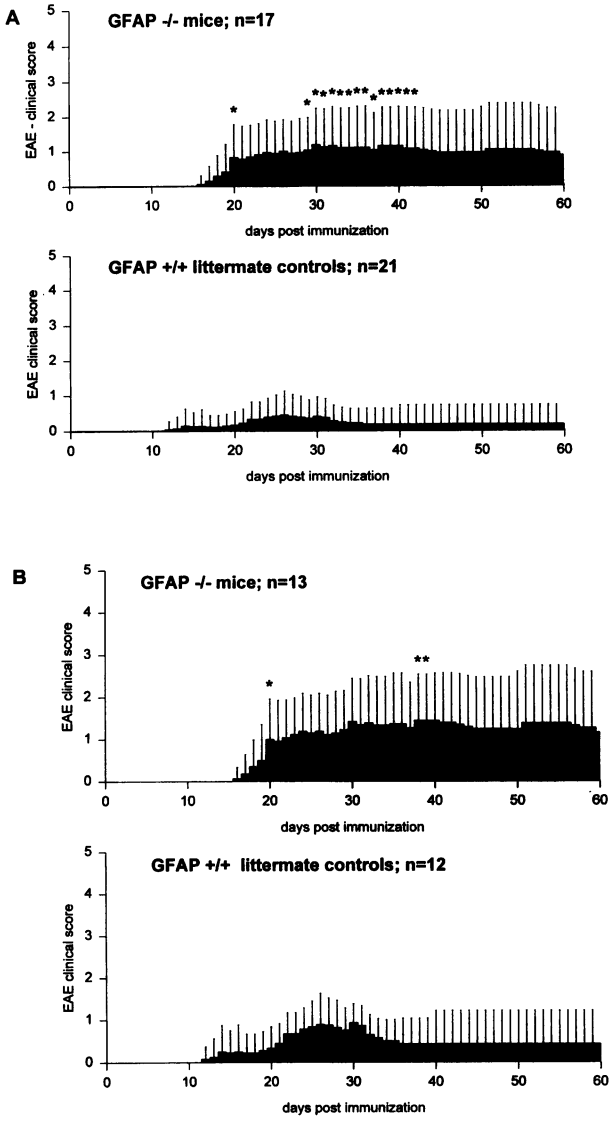

Figure 1. Clinical course of EAE in $GFAP^{-/-}$ mice and wt littermates. **A:** Clinical course is shown for all animals after immunization. * denotes statistically significant differences ($P < 0.05$, Mann-Whitney U test for comparison between groups). Note that the *P* value was 0.0507 for days 21 to 28, and that on day 43 after immunization, four animals in each group (the most severely affected) were sampled. For details on EAE clinical score, see Materials and Methods. **B:** The clinical course is shown for diseased animals only.

Electron Microscopy

A unique pattern of ultrastructural abnormalities in $GFAP^{-/-}$ CNS comprises incomplete gliosis, decreased numbers of astrocytic hemidesmosomes, and increased remyelination by immature oligodendroglia. The lack of a well-defined edge to the EAE lesion in $GFAP^{-/-}$ animals was also apparent at the ultrastructural level. On closer

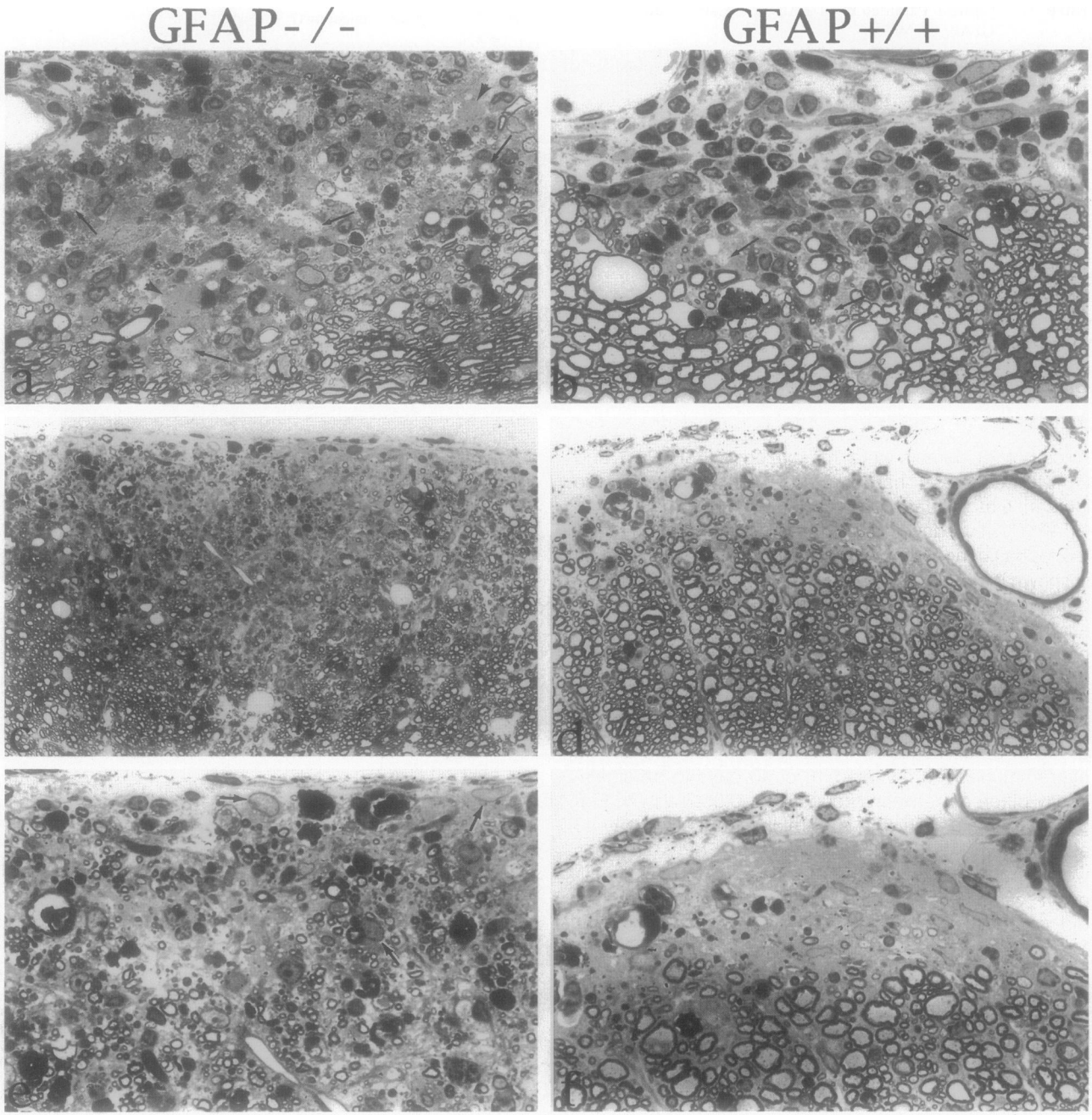

Figure 2. Light micrographs of toluidine-blue stained 1-μm epoxy sections. **a:** $GFAP^{-/-}$, acute EAE, clinical grade 1.5, day 25 after immunization. The anterior column of the lumbar spinal cord contains an inflammatory demyelinated lesion (axons at **arrows**) that comprises lymphocytes, mononuclear cells, and polymorphonuclear leukocytes within a background of reactive astrocytes with rounded cell bodies (**arrowheads**). Note the ill-defined edge to the lesion. Magnification, ×800. **b:** $GFAP^{+/+}$ littermate, acute EAE, clinical grade 1.0, day 25 after immunization. A typical EAE lesion is seen in the subpial white matter in the lumbar spinal cord. Note the demyelinated axons (**arrows**) and the clear definition to the inflammatory lesion. Magnification, ×800. **c:** $GFAP^{-/-}$, chronic EAE, clinical grade 1.0, day 60 after immunization A long-standing demyelinated lesion has an ill-defined edge. Magnification, ×220. **d:** $GFAP^{+/+}$, chronic EAE, clinical grade 1.0, day 60 after immunization. A well-demarcated chronic EAE lesion is seen around the subpial margin of the lumbar spinal cord. Magnification, ×200. **e:** Higher magnification of **c** to show the abundance of myelin droplets, fibers undergoing wallerian degeneration, and rounded astrocytes (**arrows**). Magnification, ×800. **f:** Higher magnification of **d** to illustrate the clear-cut edge of the lesion. Note how the astrocytes are tightly packed with processes radiating into the underlying white matter. Magnification, ×800

examination, the inflamed parenchyma was more loosened and edematous in $GFAP^{-/-}$ mice than in wt littermates (Figure 3, a and b). This might have been due to the stump-like $GFAP^{-/-}$ astrocytic processes that were longer than those seen in unchallenged animals but shorter than those in wt littermates, which was most apparent by immunocytochemistry, see Figure 4h (see below). Surprisingly, there was substantial fibrillary astrogliosis in $GFAP^{-/-}$ mice, which was, however, less intense when compared with wt littermates (Figure 3, a and b). In the latter, fibrillary astrogliosis did not reach the level observed in relapsing-remitting EAE in susceptible

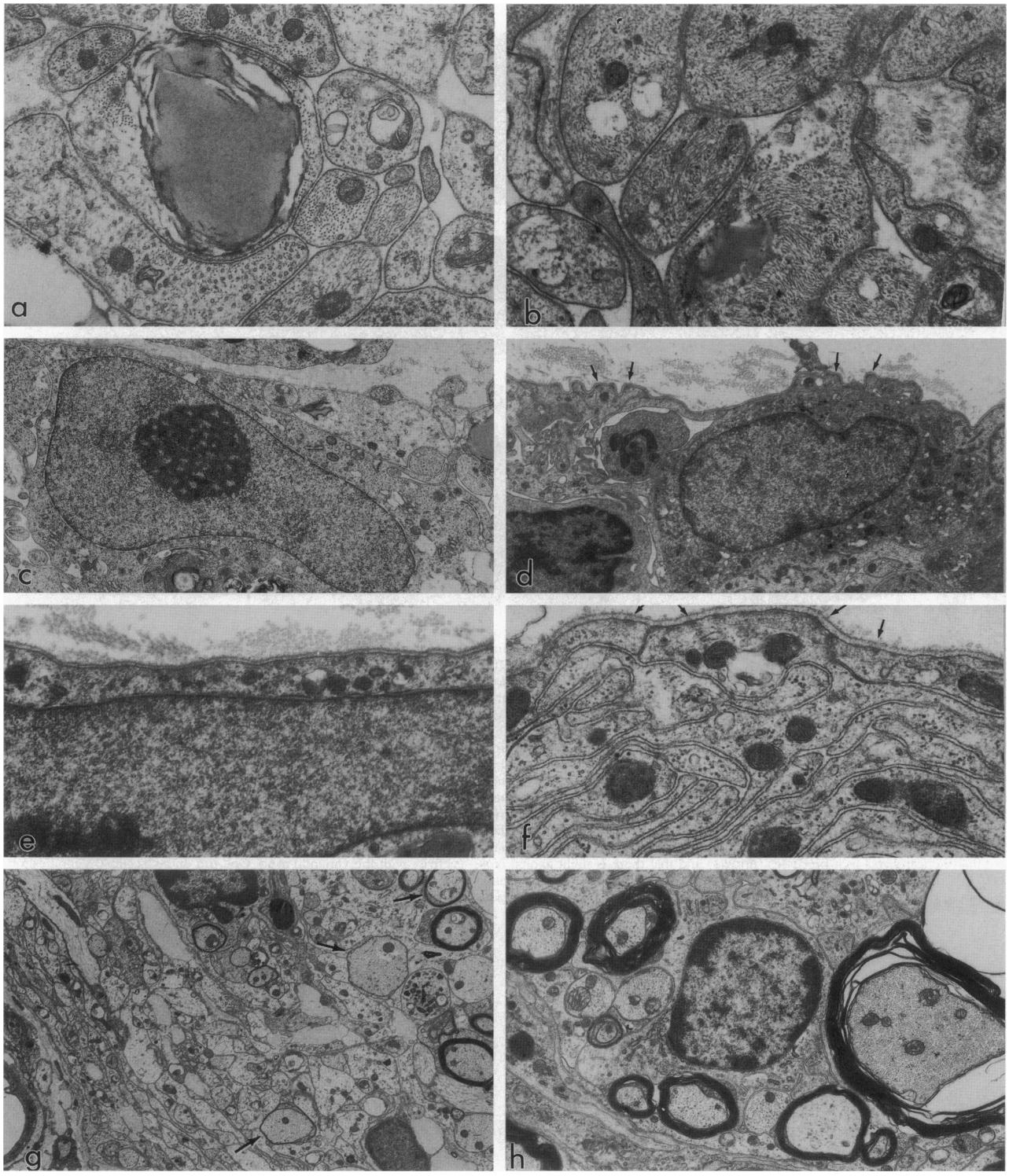

Figure 3. Electron micrographs from the CNS of $GFAP^{-/-}$ and $GFAP^{+/+}$ mice with long-standing EAE. **a:** $GFAP^{-/-}$ subpial spinal cord. Note the presence of IF in astrocyte processes that are more widely spaced than normal. One astrocyte process contains a large lipid droplet. Magnification, ×40,000. **b:** $GFAP^{+/+}$ subpial spinal cord. In this field of fibrous astrogliosis, note the abundance of IF in the closely packed astrocyte processes. Magnification, ×25,000. **c:** $GFAP^{-/-}$, a subpial astrocyte within a loosely packed parenchyma forms part of the glia limitans, which lacks membrane specializations (hemidesmosomes). Magnification, ×8000. **d:** $GFAP^{+/+}$, in this wt animal, a subpial astrocyte forms part of the glia limitans, which shows numerous hemidesmosomes (**arrows**). Note the densely packed parenchyma and the two inflammatory cells (**left**) that have invaded the tissue. Magnification, ×6000. **e:** $GFAP^{-/-}$, detail of **c**, to show the glia limitans comprising an astrocyte membrane lacking hemidesmosomes beneath a basal lamina. Magnification, ×25,000. **f:** $GFAP^{+/+}$, detail from an area adjacent to **d**, to show the abundance of hemidesmosomes (**arrows**) beneath the basal lamina of the glia limitans in this wt animal. Note how the astrocyte processes are tightly packed. Magnification, ×21,000. **g:** $GFAP^{-/-}$, an area of subpial white matter contains myelinated, demyelinated, and remyelinated (**arrows**) nerve fibers. The area of remyelination is quite extensive. Magnification, ×5000. **h:** $GFAP^{-/-}$, a cell with an immature phenotype extends short processes. The nucleus is similar to that of an oligodendrocyte. Magnification, ×7500

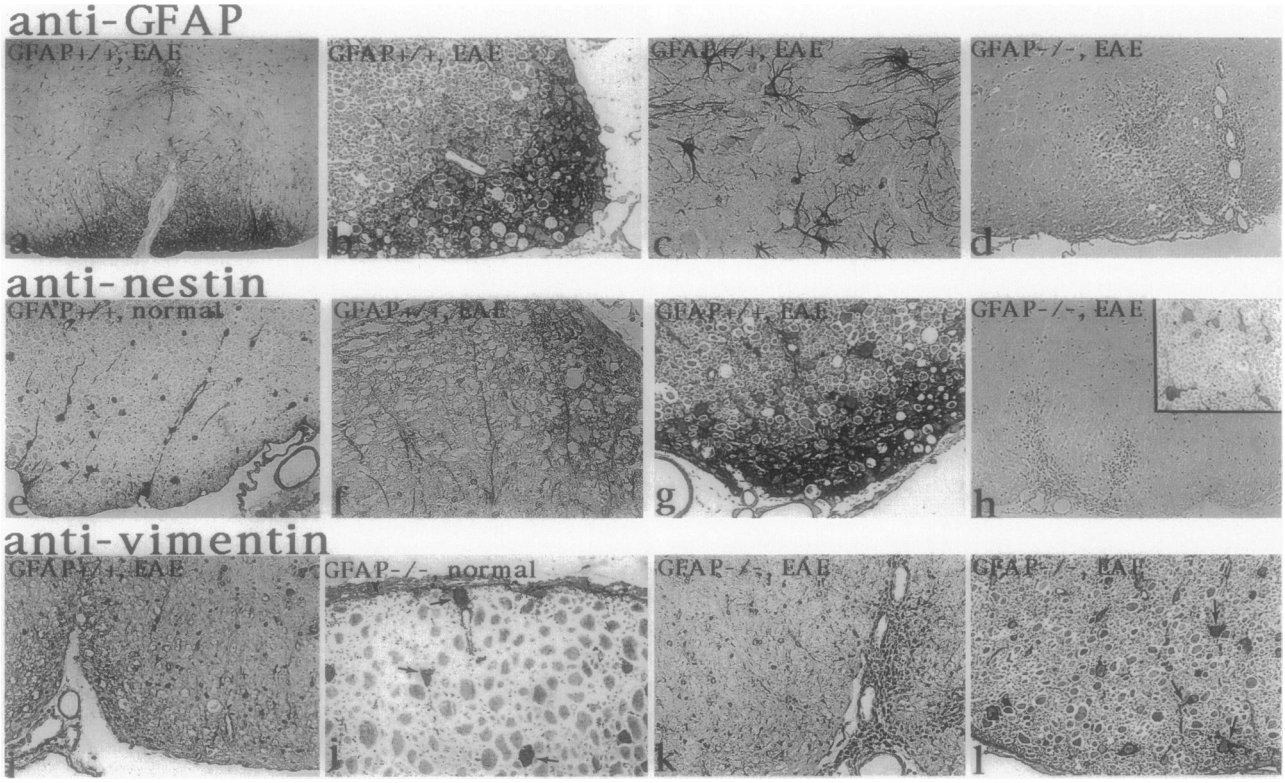

Figure 4. Astrocyte protein expression in GFAP$^{-/-}$ and GFAP$^{+/+}$ mice—spinal cord immunohistochemistry. All micrographs were taken from animals sampled on day 43 or day 60 after immunization. The first row (**a** through **d**) shows findings for GFAP-specific staining, the second row (**e** through **h**) shows those for nestin-specific staining, and the third row (**i** through l)shows those for vimentin. The type of animal is indicated on the micrograph as well as whether the tissue was sampled from EAE or normal animals. All sections were lightly counterstained with hematoxylin. **a:** GFAP-IR is shown in the EAE lesion as well as in adjacent white and gray matter. Formalin-fixed, paraffin-embedded section. Magnification, ×60. **b:** Prominent staining for GFAP is apparent in the EAE lesion. One-μm epoxy section. Magnification, ×220. **c:** GFAP-IR is shown in reactive astrocytes in gray matter far from the EAE lesion. Formalin-fixed, paraffin-embedded section. Magnification, ×600. **d:** No GFAP-IR is demonstrated in and around the EAE lesion in a GFAP$^{-/-}$ animal. Formalin-fixed, paraffin-embedded section. Magnification, ×100. **e:** Constitutive expression of nestin is apparent in radial astroglia and CNS vessels in the spinal cord of a wt animal (no EAE). This finding is in line with a recent report.[22] One-μm epoxy section. Magnification, ×200. **f:** Enhanced expression of nestin in a GFAP$^{+/+}$ animals is apparent in radial astroglia and the subpial EAE lesion. Formalin-fixed, paraffin-embedded section. Magnification, ×400. **g:** Nestin is expressed in the EAE lesion and in reactive astrocytes in adjacent white matter of a GFAP$^{+/+}$ animal. One-μm epoxy section. Magnification, ×400. **h:** Sparse expression of nestin in a GFAP$^{-/-}$ EAE lesion. **Insert:** In white matter remote from the lesion, reactive astrocytes that stain positively for nestin can be observed. Formalin-fixed, paraffin-embedded section. Magnification, ×100. **Insert:** One-μm epoxy section. Magnification, ×400. **i:** Moderately up-regulated IR for vimentin in a GFAP$^{+/+}$ EAE lesion is demonstrated. Formalin-fixed, paraffin-embedded section. Magnification, ×220. **j:** GFAP$^{-/-}$ animal (no EAE) shows constitutive expression of vimentin in subpial astrocytes and glia limitans. Note that the astrocytes lack processes (**arrows**) and that there is slight axonal cross-reactivity with the vimentin-mAb. One-μm epoxy section. Magnification, ×600. **k:** Vimentin-IR is shown in and around an EAE lesion in a GFAP$^{-/-}$ animal. Formalin-fixed, paraffin-embedded section. Magnification, ×220. **l:** Reactive, vimentin^{+} astrocytes with processes (**arrows**) are depicted in GFAP$^{-/-}$ EAE spinal cord. One-μm epoxy section. Magnification, ×400

strains of mice[16] probably due to the milder clinical score in these relatively EAE-resistant animals. Another unexpected finding in GFAP$^{-/-}$ astrocytes was the presence of a disorganized cytoarchitecture due to the irregular spacing and decreased number of hemidesmosomes, a common membrane specialization of the astrocytic glia limitans[21] (Figure 3, c to f). The paucity of hemidesmosomes was also present in unchallenged animals but was more accentuated during EAE in GFAP$^{-/-}$ mice (results not shown). Finally, there was clear ultrastructural evidence for increased remyelination in GFAP$^{-/-}$ mice with EAE (Figure 3g) in comparison with GFAP$^{+/+}$ animals, a feature in line with the previous observation of immature oligodendroglia and ongoing CNS myelination in normal adult GFAP$^{-/-}$ mice.[13] In these areas of remyelination, cells with the structural phenotype of immature oligodendrocytes were readily apparent (Figure 3h).

IF Protein Expression

Incomplete gliosis in GFAP$^{-/-}$ animals involves vimentin and contrasts to the expression of GFAP and nestin in reactive GFAP$^{+/+}$ astrocytes. The observation of fibrillary astrogliosis in long-standing EAE lesions in both groups of animals prompted us to analyze the gliotic response in the spinal cord, the prime target in EAE, by IHC and immunoblotting specific for GFAP, nestin and vimentin. By both methods, GFAP proved to be the major protein of the astrogliotic reaction in wt littermates. It occurred in intensely-stained, densely-packed astrocyte processes in and around the EAE lesion and also in hypertrophic astrocytes in gray and white matter remote from the lesion (Figure 4, a to c). Semiquantitative scoring of GFAP immunoreactivity (IR) correlated with disease activity (Table 2). As expected, GFAP-IR was absent in GFAP$^{-/-}$

Table 2. Protein Expression—Immunohistochemistry Semiquantitative Grading of $GFAP^{-/-}$ and $GFAP^{+/+}$ Mice with EAE

Animal/ IHC for:	$GFAP^{-/-}$		$GFAP^{+/+}$	
	Clinical grade*	Immunoreactivity†	Clinical grade	Immunoreactivity
GFAP	2	0	2	3
	2	0	1.5	3
	0 (+ histopath.)	0	0 (+ histopath.)	1
	0 (no histopath.)	0	0 (no histopath.)	0
Nestin	2	1	2	3
	2	1	1.5	3
	0 (+ histopath.)	0	0 (+ histopath.)	1.5
	0 (no histopath.)	0	0 (no histopath.)	1
Vimentin	2	3	2	2
	2	3	1.5	1.5
	0 (+ histopath.)	2	0 (+histopath.)	1
	0 (no histopath.)	1	0 (no histopath.)	0.5

*Clinical grade: see Materials and Methods. Clinical grade 0 (+ histopath.) denotes a clinically unconspicuous animal where CNS inflammation was present in the spinal cord. Clinical grade 0 (no histopath.) denotes a clinically inconspicuous animal without histopathological evidence for inflammation.

†Immunoreactivity values were determined by blinded observers on a scale from 0 to 4 based on density of positively stained cells and their processes. Each value stem from at least seven levels of spinal cord from a single animal (Materials and Methods).

mice (Figure 4d). In keeping with this were the results of Western blotting (Figure 5a) that showed increasing expression of GFAP with clinical severity *versus* absence of GFAP in $GFAP^{-/-}$ mice.

As a second marker for the astrocytic response during chronic inflammation, nestin was demonstrated to be present in $GFAP^{+/+}$ animals. By IHC, nestin-IR was sparse in unchallenged animals and up-regulated during EAE (Figure 4, e to g). By IHC, GFAP was expressed more abundantly than nestin. Nestin-positive astrocyte processes and reactive astrocytes were located mostly in and around lesions. Within the lesion, the localization of nestin-IR was similar to GFAP-IR (Figure 4, b and g). As with GFAP, clinical activity correlated with semiquantitative grading for nestin-IR (Table 2). In $GFAP^{-/-}$ animals with EAE, nestin played a minor role (Figure 4h); however, some nestin-positive, process-bearing reactive astrocytes could be detected (Figure 4h, insert). In comparison with unchallenged $GFAP^{-/-}$ animals, up-regulation of nestin expression and induction of process formation was noted in agreement with the ultrastructural findings. By Western blotting, the amount of nestin was increased in $GFAP^{+/+}$ animals and was gradually enhanced with clinical severity (Figure 5b). This particular correlation could also be observed in $GFAP^{-/-}$ mice but the intensity of the bands was reduced when compared with those of wt littermates. In the mouse samples analyzed, we could not detect the >200-kd nestin band. To rule out that this was associated with the 8 mol/L urea protein extraction method, we included rat pup cerebellum and spinal cord tissue from a mouse with chronic-relapsing EAE as positive controls. From these specimens, the Triton X-100-insoluble, cytoskeletal protein fraction was extracted, taking great care to avoid proteolysis. The rat sample yielded one specific band of 240 kd, whereas the EAE mouse spinal cord gave the observed pattern present in all other mouse samples. For murine protein, a major band of 130 kd was prominent. On 10% gels (nestin was routinely run on 6% gels), an additional 90-kd band became apparent, which was weaker than the 130-kd band. These blotting patterns were identical regardless of the nestin-antibody used (see Materials and Methods). These results can be interpreted as indicative of particular sensitivity of mouse nestin to specific proteolysis or as posttranscriptional processing of mouse nestin. Alternative splicing of nestin mRNA is less likely because Northern blots specific for mouse nestin have not yielded a pattern of alternatively-spliced mRNA (Dr. R. McKay, the National Institutes of Health, personal communication).

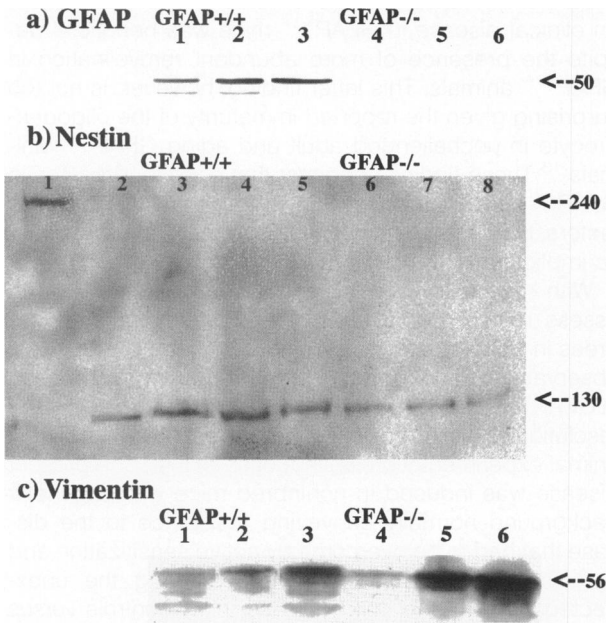

Figure 5. Spinal cord IF protein expression—Western blotting. **a:** Western blotting for GFAP. Ten μg of EAE spinal cord protein of animals sampled on day 43 or day 60 were loaded on the sodium dodecyl sulfate-polyacrylamide gel electrophoresis gel, blotted and immunodetected. **Lanes 1** to **3:** $GFAP^{+/+}$ animals and **lanes 4** to **6:** $GFAP^{-/-}$ animals. **Lanes 1** and **4,** clinical grade 0; **lanes 2** and **5,** clinical grade 1; **lanes 3** and **6,** clinical grade 2. **b:** Western blotting for nestin. Sixty μg of protein were loaded. **Lane 1:** p3 rat pup cerebellum (positive control, see text). **Lane 2:** Chronic-relapsing EAE mouse (SJL/J) spinal cord (positive control, see text). **Lanes 3** to **5:** $GFAP^{+/+}$ animals with EAE. **Lanes 6** to **8:** $GFAP^{-/-}$ animals with EAE. **Lanes 3** and **6:** Clinical grade 2. **Lanes 4** and **7:** Clinical grade 1. **Lanes 5** and **8:** Clinical grade 0. **c:** Western blotting for vimentin. Fifty μg of protein were loaded. Lanes and clinical grades as in **a.**

Table 3. Protein Expression—Densitometry of Western Blots

Western blotting	GFAP$^{-/-}$ Clinical grade	GFAP$^{-/-}$ Densitometry	GFAP$^{+/+}$ Clinical grade	GFAP$^{+/+}$ Densitometry
GFAP	2	0	2	171
	1	0	1	156
	0	0	0	80
Nestin	2	59	2	128
	1	50	1	122
	0	37	0	89
Vimentin	2	207	2	140
	1	180	1	74
	0	42	0	50

One animal per clinical grade, 8 mol/L urea protein extract from spinal cord.

The main IF of astrocytes in GFAP$^{-/-}$ mice with EAE was vimentin. In these animals, specific staining for vimentin demonstrated an astrogliotic response that was less intense than that seen in wt littermates. As mentioned above for the occasional nestin-positive GFAP$^{-/-}$ reactive astrocyte, vimentin staining confirmed the induction of process formation in GFAP$^{-/-}$ astrocytes (Figure 4, j to l). Semiquantitative grading of vimentin-IR matched the clinical activity in GFAP$^{-/-}$ animals (Table 2). In wt littermates, vimentin was found to be present in and around lesions, but when compared with GFAP and nestin, it was not more than an ancillary marker of gliosis (Figure 4i, Table 2). Western blotting for vimentin confirmed the results obtained by IHC (Figure 5c).

Densitometry of the bands in the Western blots confirmed the findings obtained by IHC (Tables 2 and 3).

Specific staining for the IF desmin and all other controls were negative.

Discussion

In the present investigation, we have induced EAE in GFAP$^{-/-}$ mice and wt littermates in an attempt to explore further the role of GFAP in CNS inflammation and in reactive fibrillary astrogliosis. Unexpectedly, in GFAP$^{-/-}$ animals, a more severe clinical course of EAE was observed, which, at the neuropathological level, was associated with an infiltrative EAE lesion. Reactive fibrillary astrogliosis in GFAP$^{-/-}$ animals involved vimentin expression and was less intense than gliosis in wt littermates in which GFAP and nestin were operative.

On closer examination, the infiltrative nature of the EAE lesion in GFAP$^{-/-}$ mice appeared to be linked mechanistically to the worsened clinical course. This tenet was supported by a lack of significant neuropathological differences. Ultrastructural pathology of the inflamed CNS in GFAP$^{-/-}$ animals added further weight to the concept that structural stabilization of the white matter through filament-competent astrocytes is a crucial factor in restricting the EAE lesion and clinical disease. GFAP$^{-/-}$ astrocytes appeared impaired in generating an effective fibrillary response to inflammation as evidenced by their poorly developed processes. Furthermore, their membrane pathology comprising irregularly-spaced and less abundant hemidesmosomes could be identified as a likely contributor to a defect in white matter structural stability. Hence, one can deduce from these observations that elaboration of astrocytic processes, as well as abundance and regularity of hemidesmosomes, are dependent on the expression of GFAP. With regard to a worsened clinical course in GFAP$^{-/-}$ mice, one might argue that more severe clinical activity may have been caused by increased production of proinflammatory mediators by GFAP$^{-/-}$ astrocytes rather than through decreased structural support that these cells contribute to inflamed white matter. Although this cannot be refuted with certainty, the observed pattern of pathology, ie, equal indices for cellular inflammation, demyelination, and even increased remyelination in GFAP$^{-/-}$ mice, argues against such an assumption. The structural role of reactive fibrillary astrocytes during inflammation might be regarded as beneficial. In the case of GFAP$^{+/+}$ astrocytes an increased expression of the IF proteins GFAP and nestin was associated with a less severe clinical course and an increased ability of the white matter to form an edge to the EAE lesion. The two patterns of reactive fibrillary astrocytosis, involving GFAP and nestin in wt animals *versus* vimentin in GFAP$^{-/-}$ mice, allow yet another interesting line of reasoning, ie, that the increased expression of nestin is ultimately dependent on GFAP expression. These positive clinical effects of GFAP expression outweigh the eventual down-regulation by glial fibrillary scarring of regenerative efforts seen in the usual demyelinated lesion of chronic EAE. The net effect on clinical disease in GFAP$^{+/+}$ mice was beneficial despite the presence of more abundant remyelination in GFAP$^{-/-}$ animals. This latter finding, however, is not too surprising given the reported immaturity of the oligodendrocyte in unchallenged adult and aging GFAP$^{-/-}$ animals.[13] These findings suggest that oligodendrocytes in GFAP$^{-/-}$ mice are driven by yet to be identified trophic factors, the characterization of which may have therapeutic implications in the future.

With regard to the light microscope methodology to assess remyelination, which revealed comparable degrees in both groups, it was clear from the ultrastructural observations that the more extensive remyelination seen in GFAP$^{-/-}$ mice by electron microscopy was beyond the resolution of 1-μm epoxy sections. From the standpoint of animal experimentation, ie, induction of EAE, the present disease was induced in noninbred mice with a genetic background normally conveying resistance to the disease that had to be overcome by active sensitization and pertussis boosting. Although underscoring the unexpected outcome, ie, mild disease in wt controls *versus* more severe disease in GFAP$^{-/-}$ mice, it would be helpful if this result could be validated in GFAP$^{-/-}$ mice with a homogeneous EAE susceptible genetic background.

Other investigators have subjected GFAP$^{-/-}$ or other transgenic mice to different procedures in attempts to induce reactive gliosis. Gomi et al[9] induced scrapie in GFAP$^{-/-}$ mice. Reactive astrocytosis could be demonstrated in knockout and wt animals as indicated by GFAP-IR in wt littermates and by lacZ-expression in GFAP$^{-/-}$ mice where the lacZ-gene was part of the trans-

genic construct. These authors noted a slightly different morphology of GFAP$^{-/-}$ reactive astrocytes in terms of vimentin-IR, namely that vimentin-staining was granular and scarce around the nucleus. These findings contrast with the present data on paraffin sections, a difference either due to methodological differences of IHC or due to the different gliosis-inciting stimuli. However, our results on 1-μm plastic sections clearly showed that astrocytic somata and processes displayed a homogeneous reactivity for vimentin in GFAP$^{+/+}$, as well as GFAP$^{-/-}$ animals. Pekny et al[10] observed reactive gliosis after cerebral stab wound in GFAP$^{-/-}$ animals. The reactive cells stained positively for vimentin and had cytoplasmic processes as was the case in the present study. Galou et al[22] observed reactive astrocytosis in vimentin$^{-/-}$ mice after cerebral stab wound. Interestingly, in this report, there was a subpopulation of vimentin$^{-/-}$ astrocytes that did not up-regulate GFAP-IR. These cells were located close to the lesion precisely where vimentin-GFAP double-positive astrocytes were detected in vimentin$^{+/+}$ mice. The authors concluded that vimentin was necessary for the appearance of GFAP-IR in a subpopulation of astrocytes and hypothesized that this was due to post-transcriptional regulation. In another study, Frisen et al[23] induced a mechanical lesion in rat and mouse spinal cord and observed reactive fibrillary astrocytosis involving GFAP and nestin. The above studies bespeak the ability of GFAP$^{-/-}$ astrocytes to respond to mechanical trauma and in the spongiform encephalopathies. They also underscore the need to study reactive fibrillary astrogliosis in GFAP$^{-/-}$ animals in other models, like the present study on CNS inflammation. In addition, these investigations reemphasize the need to examine during reactive fibrillary gliosis both detailed astrocyte morphology and protein expression of the three major astrocytic IF, GFAP, vimentin, and nestin. As highlighted by the above study by Galou et al,[22] our results are in line with the notion that IF expression after an insult is an effectively regulated event, perhaps with mutual feedback mechanisms among the three major IF in this scenario. With regard to the role of GFAP in the clinical course of EAE and in the formation of an edge to the lesion, to the best of our knowledge, there are no previous studies.

Taken in concert, the present findings highlight novel roles for GFAP during CNS inflammation, namely, the modification of the clinical course of EAE, a model for MS, and the maintenance of a well-defined edge to the white matter lesion. Furthermore, GFAP was necessary for the complete co-expression of nestin in the fibrillary astrogliotic response. These unexpected findings advance the understanding of the role of IF and astrocytes in CNS inflammation and reactive fibrillary astrogliosis.

Acknowledgments

We thank Drs. R. McKay, D. Weinstein, N. Cowan, and D. Aquino for helpful comments and suggestions; H. Finch, E. Swanson, M. Pakingan, J. Bermudez, and N. Patel for expert technical assistance; and Patricia Cobban-Bond for secretarial assistance.

References

1. Fuchs E, Weber K: Intermediate filaments: structure, dynamics, function, and disease. Annu Rev Biochem 1994, 63:345–382
2. Steinert PM, Steven AC, Roop DR: The molecular biology of intermediate filaments. Cell 1985, 42:411–420
3. Lendahl U, Zimmermann LB, McKay RDG: CNS stem cells express a new class of intermediate filament protein. Cell 1990, 60:585–595
4. Oblinger MM, Kost SA, Singh LD: Regulation of type III intermediate filament protein genes in astrocytes during development and after injury. Biology and Pathology of Astrocyte-Neuron Interactions. Edited by S Federoff, BMJ Juurlink, R Doucette. New York, Plenum Press, 1993, pp 291–302
5. Jessen KR, Morgan L, Stewart HJ, Mirsky R: Three markers of adult non-myelin forming Schwann cells, 217c (Ran-1), A5E3 and GFAP: development and regulation by neuron-Schwann cell interactions. Development 1990, 109:91–103
6. Jessen KR, Mirsky R: Astrocyte-like glia in the peripheral nervous system: an immunohistochemical study of enteric glia. J Neurosci 1983, 3:2206–2218
7. Eng LF, Vanderhaeghen JJ, Bignami A, Gerstl B: An acidic protein isolated from fibrous astrocytes. Brain Res 1971, 28:351–354
8. Eng LF, Ghirnikar RS: GFAP and astrogliosis. Brain Pathol 1994, 4:229–237
9. Gomi H, Yokoyama T, Fujimoto K, Ikeda T, Katoh A, Itoh T, Itohara S: Mice devoid of the glial fibrillary acidic protein develop normally and are susceptible to scrapie prions. Neuron 1995, 14:29–41
10. Pekny M, Leveen P, Pekna M, Eliasson C, Berthold C-H, Westermark B, Betsholtz C: Mice lacking glial fibrillary acidic protein display astrocytes devoid of intermediate filaments but develop and reproduce normally. EMBO J 1995, 14:1590–1598
11. McCall MA, Gregg RG, Behringer RR, Brenner M, Delaney CL, Galbreath EJ, Zhang CL, Pearce RA, Chiu SY, Messing A: Targeted deletion in astrocyte intermediate filament (GFAP) alters neuronal physiology. Proc Natl Acad Sci USA 1996, 93:6361–6366
12. Shibuki K, Gomi H, Chen L, Bao S, Kim JJ, Wakatsuki H, Fujisaki T, Fujimoto K, Katoh A, Ikeda T, Chen C, Thompson RF, Itohara S: Deficient cerebellar long term depression, impaired eyeblink conditioning, and normal motor coordination in glial fibrillary acidic protein mutant mice. Neuron 1996, 16:587–599
13. Liedtke W, Edelmann W, Bieri PL, Chiu FC, Cowan NJ, Kucherlapati R, Raine CS: GFAP is necessary for the integrity of CNS white matter architecture and long-term maintenance of myelination. Neuron 1996, 17:607–615
14. Martin R, McFarland HF, McFarlin DE: Immunological aspects of demyelinating diseases. Annu Rev Immunol 1992, 10:153–187
15. Raine CS: The Dale E. McFarlin Memorial Lecture: the immunology of the multiple sclerosis lesion. Ann Neurol 1994, 36:561–572
16. Raine CS: The lesion in multiple sclerosis and chronic relapsing EAE—a structural comparison. Multiple Sclerosis: Clinical and Pathogenetic Basis. Edited by CS Raine, HF McFarland, WW Tourtellotte. London, Chapman & Hall, 1997, pp 243–286
17. Raine CS: The neuropathology of multiple sclerosis. Multiple Sclerosis: Clinical and Pathogenetic Basis. Edited by CS Raine, HF McFarland, WW Tourtellotte. London, Chapman & Hall, 1997, pp 151–171
18. Skundric DS, Huston K, Shaw M, Tse HY, Raine CS: Experimental allergic encephalomyelitis: T cell trafficking to the central nervous system in a resistant Thy-1 congenic mouse strain. Lab Invest 1994, 71:671–679
19. Norton WT, Poduslo SE: Myelination in rat brain: method of myelin isolation. J Neurochem 1973, 21:749–757
20. Tohyama T, Lee VM-Y, Rorke LB, Marvin M, McKay RDG, Trojanowski JQ: Nestin expression in embryonic human neuroepithelium and in human neuroepithelial tumor cells. Lab Invest 1992, 66:303–313
21. Fuchs E: Keith R Porter Lecture, 1996, Of mice and men: genetic disorders of the cytoskeleton. Mol Biol Cell 1997, 8:189–203
22. Galou M, Colucci-Guyon E, Ensergueix D, Ridet J-L, Giminez y Ribotta M, Privat A, Babinet C, Dupouey P: Disrupted GFAP network in astrocytes from vimentin knockout mice. J Cell Biol 1996, 133:853–863
23. Frisen J, Johansson CB, Torok C, Risling M, Lendahl U: Rapid, widespread and long lasting induction of nestin contributes to the generation of glial scar tissue after central nervous system injury. J Cell Biol 1995, 131:453–464